Enhancing the Performance of Stretchable Conductors for E-Textiles by Controlled Ink Permeation

*Hanbit Jin, Naoji Matsuhisa, Sungwon Lee, Mohammad Abbas, Tomoyuki Yokota, and Takao Someya**

Delivery of electronic functionality to the human body using e-textiles is important for realizing the future of wearable electronics. Printing is a promising process for large scale manufacturing of e-textile since it enables arbitrary patterns using a simple and inexpensive process. However, conductive inks printed atop of textile are vulnerable to cracking because of the deformable and porous structure of textiles. The authors develop a mechanically and electrically robust wiring by controlling ink permeation in the structure of textile. This is done by adjusting the ink's solvent. The use of butyl carbitol acetate, with its low vapor pressure and boiling point, enables deep permeation into the textile. The sheet resistance is initially 0.06 Ω sq^{-1}, and the resistance increasing only 70 times after stretching to 450% strain. Finally, a four-channel electromyogram (EMG) monitoring garment is demonstrated to show the potential of a large-scale e-textile device for health care and sports.

Research on textile-based electronics (e-textiles) is fueled by the pursuit of the ultimate wearable platform, comparable to clothes we wear on a daily basis. The goal of wearable e-textiles is to deliver electronic functions, such as sensing,[1–4] light illumination,[5,6] and human computer interfaces,[7] to the each part of human body by integrating electronic devices into textiles. In addition to the accessibility, comfort, and durability, the flexibility and stretchability of e-textiles are extremely important. Recently, there has been a great deal of progress in flexible and stretchable electronics, using organic/oxide semiconductors,[8–11] ultrathin silicon membranes,[12] carbon nanotubes,[13,14] silver nanowires,[15,16] and intrinsically conductive polymers.[17–19] These breakthroughs afford precise and high-resolution measurement of vitals and various physiological data, such as electrical signals,[12] pressure,[20] temperature,[21] and blood glucose.[22] By transferring these thin film devices to the surface of skin or textiles, wearable devices can take advantage of high-performance electronics, although the sensing area is small compared to the entire body surface. To scale up sensor distributions and build a truly integrated system, a popular strategy is to connect prefabricated films[23] and fiber devices[6,24] with the stretchable wirings. This approach allows a high-level integration, connecting inevitably rigid components such as microprocessors and wireless modules which enable programmable operations and wireless communications. Furthermore, the location of rigid components can be designed to be located in nondisturbing locations by extending the wires. To build a distributed large-area sensor system in a comfortably wearable textile platform, stretchable wirings that can minimize losing original mechanical properties of textile substrate is of paramount importance.

Several types of wiring methods have been demonstrated for e-textiles. One method is the embroidering, knitting, and weaving[25,26] of conductive threads into textiles. They fully utilize textile structures and enable small bending stiffness and stretchability of the resultant textile, giving reliable electrical performance against large strains. These processes are solvent-free and compatible with the conventional fabrication equipment used in the textile industry. Similar mechanical and electrical properties can be achieved by coatings. In the past, textiles have been coated by conductive materials, such as single walled carbon nanotubes,[27] conductive polymers,[28] silver nanowires,[29] and metal plating.[30] In addition to using flexible conducting structures atop textiles, taking advantage of structural motifs such as serpentine configurations in textiles allows for further improvement in electrical and mechanical performance.[30] Finally, printing processes have been suggested for wirings of e-textile. Stencil and screen printing are being widely used in both textile and electronic industries, since they provide low production cost and high throughput. To obtain stretchable wiring on textile with a printing processes, viscous composite inks of conducting filler and elastomeric binder have been prepared and printed on textile either directly[31–33] or with an interface layer.[34,35] They showed a low sheet resistance of 52.5 mΩ sq^{-1} on average when the ink

H. Jin, Dr. N. Matsuhisa, Prof. S. Lee,[+] M. Abbas, Dr. T. Yokota, Prof. T. Someya
Department of Electrical Engineering and Information Systems
University of Tokyo
7-3-1 Hongo, Bunkyo-ku, Tokyo 113-8656, Japan
E-mail: someya@ee.t.u-tokyo.ac.jp
Dr. T. Yokota, Prof. T. Someya
Exploratory Research for Advanced Technology (ERATO)
Japan Science and Technology Agency (JST)
7-3-1 Hongo, Bunkyo-ku, Tokyo 113-8656, Japan

[+]Present address: Department of Emerging Material Science, Daegu Gyeongbuk Insistute of Science & Technology (DGIST), 333, Techno Jungang-daero, Hyeonpung-myeon, Dalseong-gun, Daegu, 711-873, Korea

DOI: 10.1002/adma.201605848

was printed on different textiles,[31] and 49.4 mΩ sq^{-1} when the ink was printed on an interface layer.[35] However, printed composite materials suffer from large resistance changes under stretching and cyclic stress because of deformable porous structures of textiles. Moreover, the printed layers on top of the textile stiffen the textile by binding the fiber bundles and disturbing movement of fibers in textiles. To avoid the cracking of printed materials and stiffening the textile, the ink should coat or be contained only on the individual textile fibers, instead of filling whole cavities of textile and binding them together. Thin inks can meet this requirement, however, multistep processing is necessary for patterning, which sacrifices process simplicity and the textile's original texture.[7] Nonetheless, viscous inks do not permeate well into porous textile structures even though they are easy to be patterned on textiles.

Here, we report a textile-permeable viscous ink which can be directly screen/stencil printed on textile substrates. This conductive composite enables highly conductive and stretchable wirings on textile with a simple and inexpensive way. The resulting high stretchability (up to 450%) and low sheet resistance (0.06 Ω sq^{-1}) is due to the combined ink/textile structure formed by the permeation process. The permeation process enables the utilization of the textile's wavy structure, allowing for the fabrication of highly stretchable printed e-textiles (**Figure 1**). Although our previous ink in ref. [33] showed high stretchability up to 218% only on elastomer substrates, such a high stretchability was not reproduced on textiles. The higher stretchability and better cyclic durability have been achieved by newly developed conductive ink that is intentionally permeable in textile substrates. In order to show the feasibility of the improved durability and stretchability of our ink, we have manufactured a compression type electromyogram (EMG) monitoring system that maintains the stable contact with a skin and suppresses the motion artifact.

The stretchable conductive ink is comprised of a fluoroelastomer (poly(vinylidene fluoride-co-hexafluoropropylene),

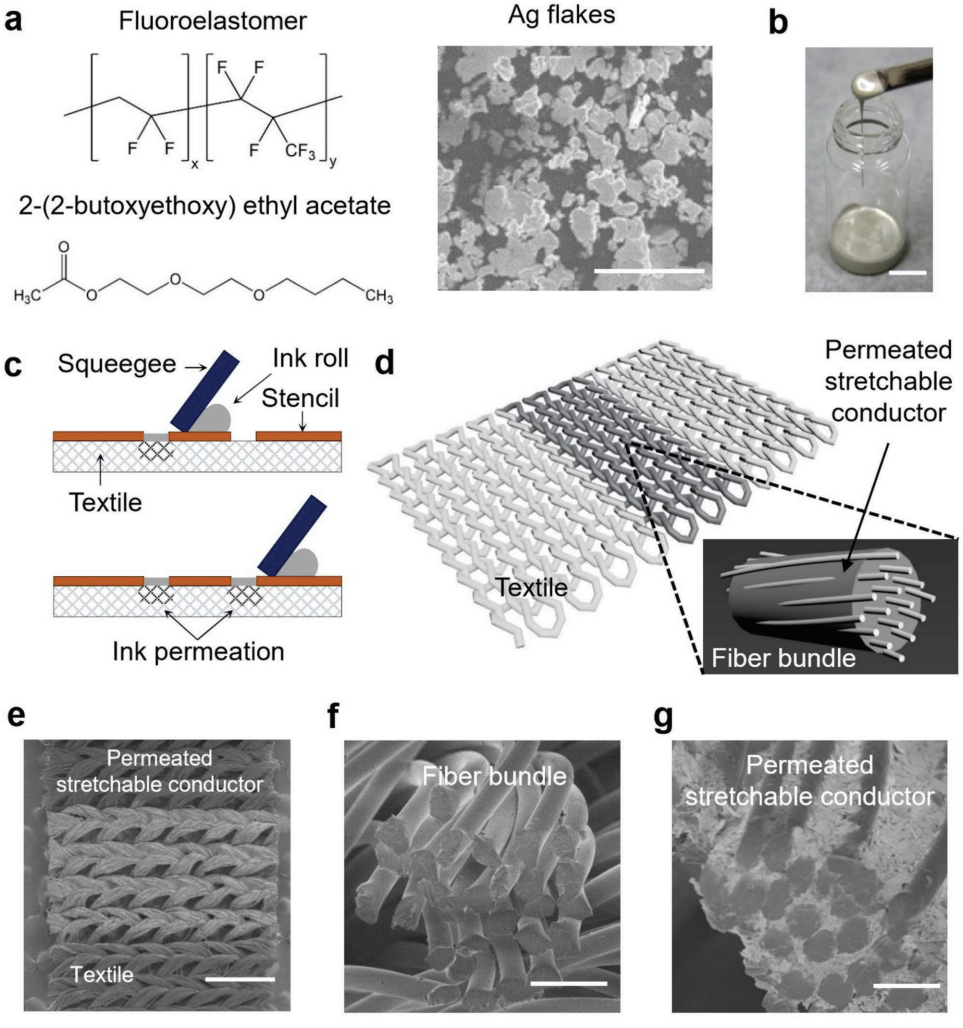

Figure 1. A textile-permeable conductive ink for stretchable printed e-textile. a) Ingredients of the silver-fluoroelastomer composite, the scale bar is 5 µm. b) As-formulated viscous ink of the silver-fluoroelastomer composite, the scale bar is 1.5 cm. c) Illustration of direct stencil printing on textile and ink permeation to a textile substrate. d) Illustration of printed stretchable wiring on the knit textile and permeated composite in a single fiber bundle. e) SEM surface image of printed stretchable wiring. Scale bar is 500 µm. f) Cross-section SEM image of the textile, before and g) after printing, respectively, the scale bars are 30 µm.

2-2(butoxyethoxy)ethyl acetate (or butyl carbitol acetate, BCA), and silver flakes with an average particle size of 2–3 μm in a weight ratio of 1:2.45:4 as shown in Figure 1a. The fluoroelastomer gives the softness and stretchability to the composite and was chosen because of its chemical and environmental stability. BCA has a high boiling point (247 °C) and low vapor pressure (<0.01 mmHg), which plays an important role for permeation of viscous inks into textile. Silver flakes are high aspect-ratio conducting filler which yields high conductivities at low volume fractions and are inexpensive compared with silver nanowires or nanoparticles. To prepare the ink, the fluoroelastomer was dissolved in BCA first and then silver flakes were added to the solution yielding a viscous ink as shown in Figure 1b. The concentration of the polymer and fraction of silver flakes determine the viscosity of the solution. The viscosity of ink was 59.2 Pa s at a 1 s^{-1} sheer rate (Figure S4, Supporting Information) which is viscous enough for screen and stencil printing.

The prepared ink was printed by a simple stencil printing process with a glass slide covered with polyimide tape acting as a squeegee and patterned using a 125 μm thick polyimide mask, directly on the textile substrate (Figure 1c). The textile was fine 30-denier tricot knit textile of nylon and polyurethane. This tricot knit textile is commonly used for underwear and sportswear because of its excellent stretchability of up to ≈450% strain and good recovery under 100% strain. The ink was squeezed onto the substrate through the mask 5 times. Printed traces were then dried at 90 °C in an oven for 2 h, followed by heat-pressing at 160 °C for 30 s at a pressure of 30 kPa.

After the stencil printing, the ink was absorbed from the surface to the inside of textile by a capillary process called "wicking" (Figure S1, Supporting Information). This phenomenon is observed in fiber bundles and has been studied to understand fluid transportation in textile and brush.[36–38] The ink is added from the surface of the textile and then carried in capillaries formed by fibers in the individual yarns. By printing the silver fluoroelastomer composite ink atop the textile, the ink permeates into the textile and is immobilized inside of the fiber bundles as the ink dries. Consequently, the stretchable conductors form intrinsically stretchable conductive paths inside of fiber bundles and fiber bundles retain the structure of knitted textile as shown in illustration (Figure 1d) and the SEM image of the surface (Figure 1e). Therefore, it can benefit from both intrinsic stretchability of the ink material and the deformable structures of the knitted textile. The fiber bundles filled with stretchable conductors was revealed by cross-sectional scanning electron microscope (SEM) images of fiber bundles before and after printing, respectively (Figure 1f,g). Even the small gaps (<10 μm) between fibers were filled with the stretchable conductor composite, and the microscale silver flakes could penetrate through the small gaps as shown in magnified SEM images (Figure S1, Supporting Information). While gaps between individual fibers were filled with the inks, the larger vacancies between the bundles of fibers were not filled with the ink because the fluid transported, permeated, and remained only in the fiber bundles. Thus, periodically interlocked loops of knit textile were not immobilized, maintaining textile's soft and stretchable mechanical properties. The tensile force for 1% deformation is just ≈5 times higher than the original textile, and is almost the same in strains greater than 40% (Figure S2, Supporting Information).

The effect of permeated ink to the textile structure was investigated by printing the ink on knitted textile and a 20 μm thick polyurethane (PU) substrate for comparison (**Figure 2**). Instead

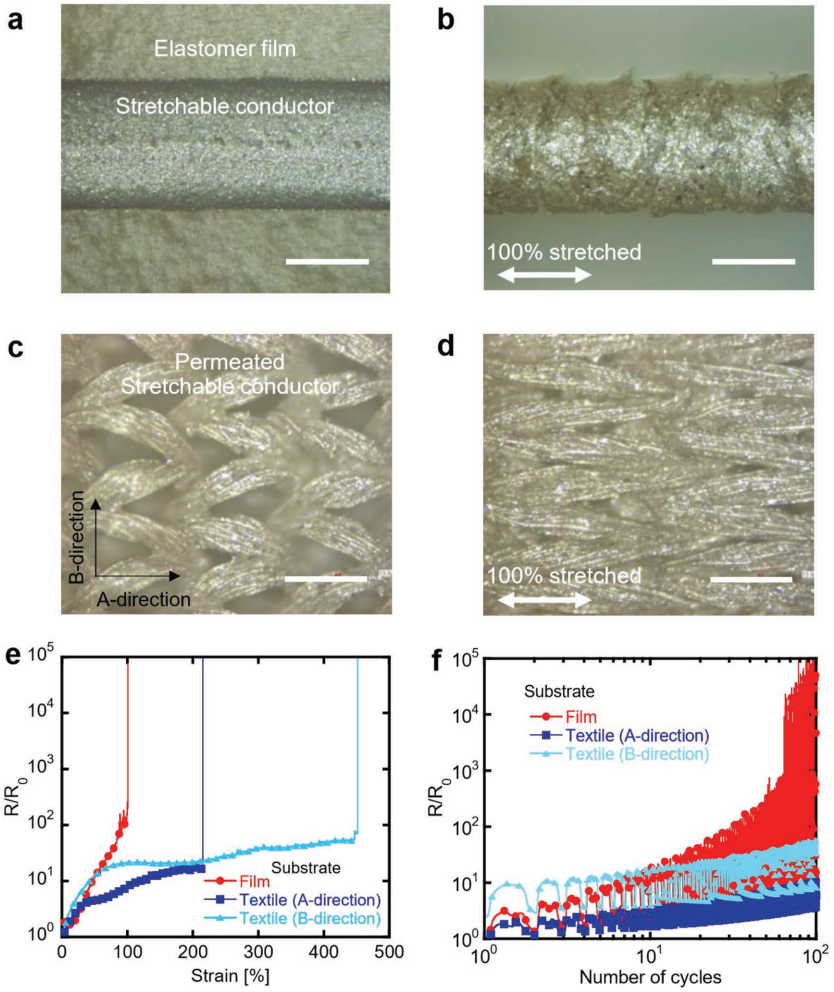

Figure 2. Comparison of film substrate and textile substrate. a) Microscopic image of silver fluoroelastomer composite printed on polyurethane film. b) Cracked silver fluoroelastomer composite on polyurethane film after 100% stretching. c) Microscopic image of silver fluoroelastomer permeated textile. d) Straightened fiber bundles at 100% strain. e) Normalized resistance changes of silver fluoroelastomer printed on polyurethane film substrate (red circle), on textile in the A-direction (parallel to fiber bundles, blue square), and the B-direction (perpendicular to fiber bundles, aqua triangle) during stretching. f) Normalized resistance change of the composite printed on film and textile during cyclic 30% strain. Scale bar is 300 μm.

of using a single yarn, PU substrate was used for comparison because of the issue of yarn's stretchability and issue of printing process on yarns. The ink formed on PU showed a stretchability up to 100%, which is an intrinsic stretchability of the printed composite. After 100% strain, printed line on PU substrate electrically disconnected because of the cracks as shown in Figure 2b. Clearly, when printing on the textile, the printed ink assumed a similar 3D structure as the underlying textile (Figure 2c,d). The knitted textile has an anisotropic structure and anisotropic strain-stress behavior (Figure S5, Supporting Information). Therefore, the direction of printed wires affects electrical and mechanical performance. Here we define the anisotropy of the textile structure as having A and B directions. The A-direction (wales) is parallel with fiber bundles, while the B-direction (courses) is perpendicular to fiber bundles (black arrows in Figure 2c). The electrical characteristics were compared under large strains of 0%–450% and cyclic 30% strains in these two directions as shown in Figure 2e,f. The dimension of printed trace was 1 mm width and 30 mm length. The relative resistance of printed line on knitted textile increased 7.87 times (A-direction) and 21.2 times (B-direction) after 100% stretching, while the resistance of printed line on polyurethane, an isotropic structure film, increased 256 times. Moreover, printed lines on textile were stretchable up to 215% (A-direction) and 450% (B-direction), while printed lines on polyurethane film were only stretchable up to 100%.

In addition to single stretches, the printed line on textile showed durable and stable electric conduction under cyclic stretching. This can be explained by microscope images of initial and stretched states as shown in Figure 2a–d. In the case of film substrate, applied strain was directly delivered to the top stretchable conductive layer, so that printed line was damaged by cracks. On the other hand, in case of textile substrates, conductive ink was well integrated with fibers and stress was relieved by deformation of the textile structure. Fiber bundles of textile have an initially curved shape that is straightened when strain is applied to the textile as shown in Figure 2c,d. This is achieved since the ink selectively fills the small gaps within each fiber bundles and fails to fill the big gaps between fiber bundles. Thus, the combination of fibers and printed materials easily comply with deformations like bending and straightening. Furthermore, resistance changes were almost negligible by the various deformations; $\Delta R = -0.1\Omega$ (5% of initial resistance), 0.3Ω (15%), 0.3Ω (15%) when 86.1 N cm^{-2} of vertical pressure, 720° twisting, and 90° folding were applied, respectively. The conducting lines printed on knitted textile showed smaller resistance change than printed lines on the isotropic and planar polyurethane substrate.

The evaporation rate of inks was found to be the dominant parameter among the properties of solvent to form the above described formation of conductive pathways in textile fibers. Solvent plays an important role that determines the rheological and drying behavior of ink solution, which determines the permeation properties, namely, surface morphology and permeation depth of printed traces on textile fibers. Here the permeation properties were investigated by printing inks with three different solvents that have different evaporation rates. They are acetone, methyl isobutyl ketone (MIBK), and BCA. The boiling point of acetone, MIBK, and BCA is 56, 117, and 246 °C and vapor pressure is 182, 16, and <0.01 mmHg at 20 °C, respectively. Here, all the inks were prepared with same volume percent of solvent and viscosity of acetone, MIBK and BCA inks were 18.3, 10.3, and 59.2 Pa s, respectively (Figure S4, Supporting Information). The inks were printed using just one pass and no heat press treatment was applied to observe the effect of permeation. **Figure 3**a–c shows the surface SEM images of printed lines on textile. Figure 3d–f shows cross-sectional images of printed ink in textile. Furthermore, permeation depth of each sample was obtained from SEM cross-sectional images as shown in Figure S5 (Supporting Information). Acetone ink (Figure 3a,d) did not permeate into textile, permeation depth of 157 μm, and formed a film on the surface of textile. As acetone evaporated fast, the ink dried before it could penetrate the deeper fiber bundles and remained near the surface of textile. The MIBK ink also formed continuous film on the surface but it permeated more than the acetone ink, permeation depth of 191 μm. The outlines of fibers were observed on surface (Figure 3b) and the permeation depth was deeper than the acetone ink (Figure 3e). On the other hand, the BCA ink showed three dimensional configurations which remained only on the fiber bundles (Figure 3c). In the cross-sectional image, this ink penetrated to the deepest region among all the inks, penetration depth of 231 μm, and reached the junction points of fibers bundles (Figure 3f).

Such permeation properties directly affect the electric performance, as observed through the resistance change during elongation, as shown in Figure 3g. The acetone ink remained near the surface of textile and showed a poor stretchability of just 35% (line with circle legend in Figure 3g). This is explained by SEM images during stretch (Figure S3, Supporting Information), which shows a cracked film on the surface of textile. On the other hand, the MIBK ink showed better stretchability yet unstable electronic performance (line with triangle legend in Figure 3g). It disconnected near 60% strain, but showed electrical conduction again at larger strain. This is explained by incomplete filling of the ink to junction points of fiber bundles, so that it is vulnerable to cracking when there is huge displacement of fiber bundles (Figure 3e). After 60% of stretching, the fiber bundles condense and make new electrical contacts between fiber bundles. Finally, fully permeated conducting traces obtained by BCA ink showed stable electrical conduction during stretching (line with square legend in Figure 3g). This is consistent with the SEM images in the relaxed and stretched conditions (Figure S3, Supporting Information), showing no cracking in the conducting composite but structural deformation of textiles. BCA ink was electrically disconnected not until 210%, limited by the maximum stretchability of textile substrate.

Not only the maximum elongation was improved, but also the cyclic durability was improved when BCA was used as solvent. Figure 3h shows cyclic durability of the conductivity of lines made using acetone (circle), MIBK (triangle), and BCA ink (square) while 10% stretching cycles applied. The resistance gradually increased with the stretching cycles and BCA showed the smallest change. Its relative resistance change was less than 10 times compared to the initial resistance after 100 cycles. With multiple passes of printing and heat press process, the cyclic durability significantly improved; 26 Ω (stretched) and 3 Ω (relaxed) after 1000 cycles.

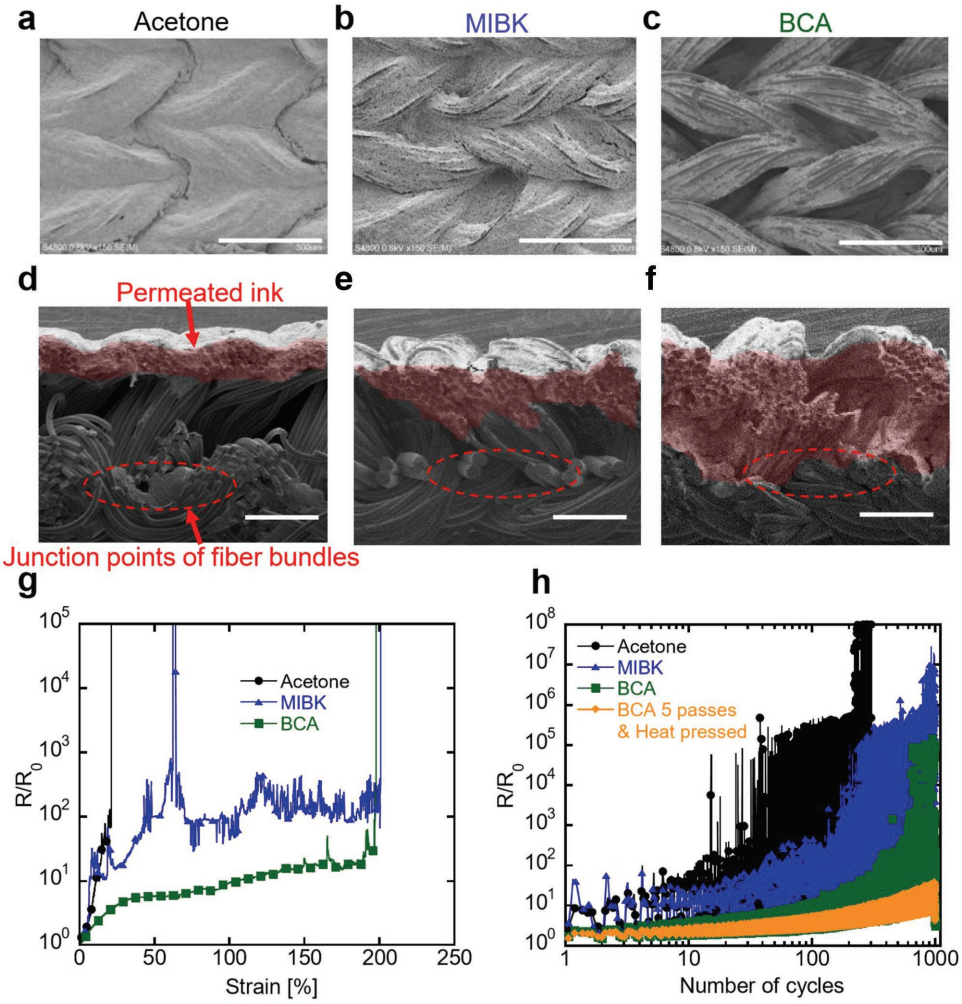

Figure 3. Permeation properties of silver fluoroelastomer composite inks which were fabricated with acetone, MIBK, and BCA solvent. SEM surface image of composite ink whose dissolving solvent was a) acetone, b) MIBK, c) BCA, scale bar is 300 µm. SEM cross-section image of d) acetone ink, e) MIBK ink, f) BCA ink, shaded red regions are permeated ink. The scale bar is 150 µm. g) Normalized resistance changes of acetone (black circle), MIBK (blue triangle), and BCA ink (green square) printed on textile during stretching. h) Normalized resistance changes of inks during cyclic 10% strain. Each sample was printed in 1 pass (acetone: black circle, MIBK: blue triangle, BCA: green square) except BCA five passes sample (yellow diamond).

The concentration of the ink was also investigated because the permeation is expected to be further improved by dilution of the ink. However, when we print the dilute composite ink on textile, the same gradient of resistance change was observed during cyclic test, but the resistance was increased (Figure S4, Supporting Information). This is because diluted ink has less solid content in the same volume than the viscous ink. The effect of silver flake fraction was also investigated, but showed minimal changes of electrical and mechanical durability (Figure S5, Supporting Information) although a clear stretchability–conductivity trade-off is observed when the ink was printed on polyurethane. Finally, the effect of printing passes and post heat-press treatment was investigated. Figure S6 (Supporting Information) describes the effect of printing-pass numbers on the cyclic durability. The number of printing passes affects the permeation to the textile structure because it is related to amount of delivered ink when the substrate absorbs the ink. In this work, five passes of printing were conducted to obtain stable electrical performance (Figure S6, Supporting Information). Heat pressing was applied as a post printing treatment to help improve the conductivity and cyclic durability (Figure S7, Supporting Information). This improvement is confirmed by SEM images, showing the silver-fluoroelastomer composite in fiber bundles become denser and the textile structure condenses after heat pressing (Figure S8, Supporting Information). Textiles were not damaged by heat press because the melting point of nylon is 220 °C and polyurethane (spandex) is 230 °C. Finally, the initial resistance of wire was as low as 0.7 Ω, and the resistance change after 1000 cycles of 10% strain is less than 35 times (Figure 3h). Although we used slow evaporating solvent (BCA), of which boiling point is 247 °C, the solvent rarely remained in the composite material. The amount of solvent residue was 0.0011 mg (0.012 wt% of the solvent in as-printed ink) after drying 2 h at 90 °C and heat pressing process (Figure S14, Supporting Information). Printed composite material showed stable electrical and mechanical properties even after 220 d in air (Figure S13, Supporting Information).

Permeation controlled inks can realize a stretchable and mechanically durable textile electrode, while permeation uncontrolled inks showed drastic or unstable resistance changes during the stretching. Fully utilizing this, a light-emitting diode (LED) integrated textile was fabricated and keep illuminating while it stretched up to 400% (Figure S9, Supporting Information). A green LED was attached to textile using epoxy and connected with printed textile electrode via conductive epoxy (Figure S9, Supporting Information). When the device is fabricated along the A-direction, the device was stretchable up to 200% until the textile tore, but had a lower resistance than the perpendicular (B) direction. When the same circuit is fabricated in the B-direction, the device was stretchable up to 400% but had a higher resistance than the parallel (A) direction (Figure S9, Supporting Information). During the stretching, the current change was recorded with a constant external voltage of 3 V to LED integrated textile. In case of the A direction which is parallel to fiber bundles, initial current was higher than the B direction which is perpendicular to fiber bundles. If we convert current to resistance (3 V is applied), net resistance of circuit changed from 278 to 492 Ω at 208% strain in A direction, and from 329 to 625 Ω at 404% strain in B direction. This stretchable LED circuit is achieved by the print-patternable, silver-based highly conductive ink. Furthermore, we investigated heat generation of printed traces when the electrical current flows through the traces. The temperature of printed traces was increased 1 °C from 26 to 27 °C when we apply 100 mA (Figure S15, Supporting Information), while maximum current of single LED is 30 mA. This would enable more sophisticated illuminated costumes or safety clothes.

Finally, an EMG monitoring system on skin-tight compression garment was demonstrated to show a potential application of the stretchable printable textile circuit as a biometric device. Stretchable transmission lines and vital electrodes were printed on textile and connected to a wireless module. After the printing and post processes, 50 μm thermoplastic polyurethane (TPU) layers were laminated on both sides of transmission lines to prevent sweat and unnecessary contacts with skin. This additional protection layer is necessary for practical uses, enduring machine washing (Figure S12, Supporting Information) and abrasion. The size of garment was designed to be 72% smaller than forearm size, namely, the diameter of the arm was 25 cm and the diameter of the sleeve was 18 cm. This compression design enabled stable contact between electrode and skin even during motion. When this compressed garment is worn on the arm, the textile and conductive traces are stretched, and the recovery force makes electrodes stay on surface of skin to maintain stable and conformal contact. As a result, noise induced by arm twists was significantly decreased when compared with the noncompression design (Figure S10, Supporting Information). A volunteer wore the compression EMG measurement garment (**Figure 4**a) and conventional Ag/AgCl gel electrode was used as a control measurement. EMG signals were measured during hand opening (rest) and closing motions. As shown in Figure 4b, EMG signals measured from the compression sleeve based device are comparable with signals from conventional Ag/AgCl gel electrode. The noise levels of the electrodes were 0.07 mV (compression) and 0.06 mV (control). Furthermore, we increased the number of channels and demonstrated four-channel EMG monitoring sleeve. Four pairs of electrodes were located on four different muscles of the fore arm and monitored muscle activation during the hand closing motion (Figure 4c,d). In addition to the original EMG signals, we provided digital processed signal in Figure S16 (Supporting Information). We could observe different activations of muscle during hand opening and closing motions. By using

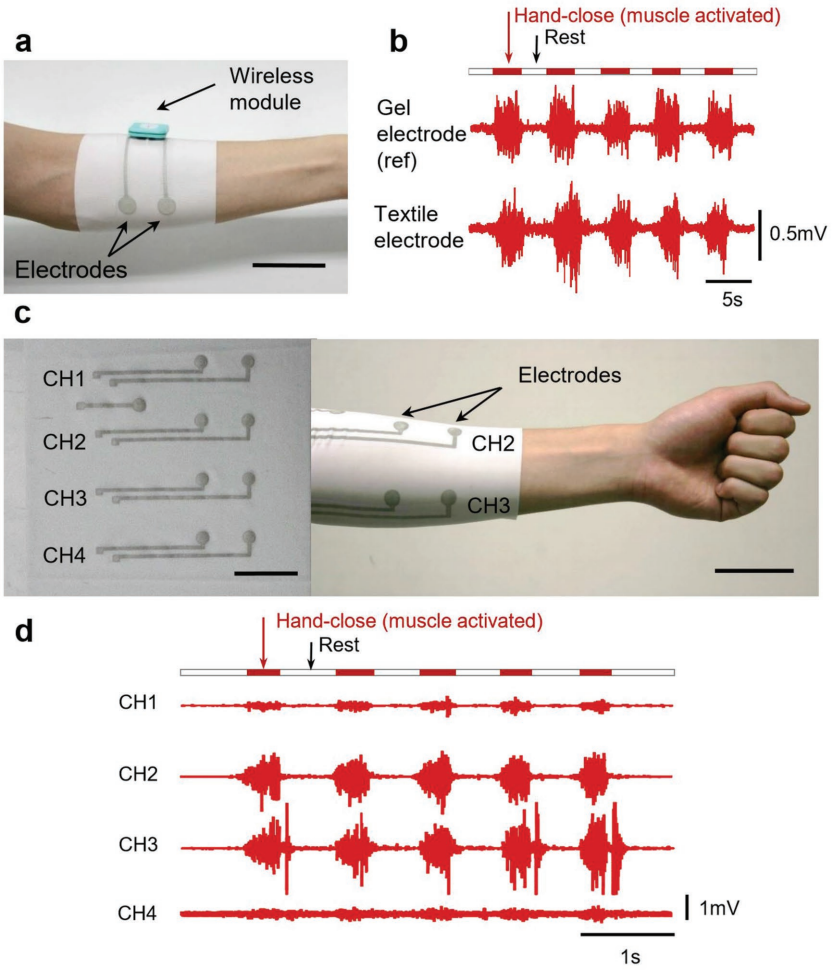

Figure 4. The skin-tight compression garments for EMG measurement. a) An image of one channel printed textile electrodes with compressive design. The scale bar is 5 cm. b) EMG signals from the fore arm measured by conventional gel electrodes and compressive textile sleeve electrodes during muscle activation and rest. c) Images of printed four-channel EMG measurement sleeve before wearing (left) and after wearing (right). Scale bars are 5 cm. d) EMG signals of fore arm muscles measured by a four-channel sleeve during hand-close (5 times) and rest.

this textile-permeable conductive ink, the sensing system on compression suit designs were realized, enabled here by high stretchability of printed composite on textile. Furthermore, the EMG measurement is customizable since the design is freely changeable. This approach largely simplifies the work to mount multielectrodes on bodies of patients or sports players, which is tough and can be uncomfortable for both workers and patients.

In this work, a textile-permeable conductive ink was developed to improve mechanical durability of printed e-textiles. The degree of permeation of the ink into the textile is important to realize stretchable wirings on textile, which benefit from intrinsic stretchability of composite and structure of textiles. Slow evaporating solvent enabled permeation of viscous ink into textile. As a result, initial sheet resistance of printed lines was 0.06 Ω sq^{-1}, and relative resistance increased only 70 times after stretching up to 450% due to the optimal morphology of textile bundles and conductive composite. This mechanically durable and simply printable composite material enabled the realization of a multichannel EMG monitoring compression garment. We anticipate that this stretchable conductive ink for textile can provide new design opportunities for wearable e-textile applications such as health monitoring garments and textile integrated sensors.

Experimental Section

Fabrication of Stretchable Conductor Inks: Fluoroelastomer (DAI-EL G801, Daikin Industries) and BCA were mixed with weight ratio of 1:2.45. After stirring with a magnetic stirrer for 12 h, silver flakes (product number: 327077 Aldrich, Silver flakes, 10 mm, >99.9% trace metal basis) were added to the solution in a 4:1 (silver:fluoroelastomer) weight ratio and mixed with magnetic stirrer for 3 h before use. For the evaluation of permeation properties of ink samples, acetone, MIBK, and BCA were used. The volume fraction of solvent was kept same (72.7 vol%). After the ink formulation, viscosity was measured by cone-plate type viscometer (TVE-25H, Toki Sangyo Co., Ltd). And cone rotor (3°R9.7, Toki Sangyo Co., Ltd) was capable of measuring viscosity range from 1.88 Pa s to 3.8 kPa s. Measurement temperature was maintained as 25 °C by circulator.

Stencil Printing of Textile Permeable Ink and Post Treatment: The conductive traces were stencil printed with 1 mm width and 40 mm length on fine knitted fabric (FR3600: 2-way stretch tricot, 30 denier Nylon 76%, 30 denier Polyurethane 24%, UTAX Co. Ltd, Japan) and a 20 µm thick polyurethane substrate (NSK Echomark, Japan). The stencil mask was made of a 125 µm thick polyimide film, cut by a green laser (MD-T1010, Keyence). A glass slide was used to spread the ink. 1–20 passes of printing were conducted to investigate the amount of ink delivery into textile, and 5 passes of printing were conducted for stretching test specimens. Subsequently, the printed textile was dried in 90 °C oven for 2 h. After the drying process, the printed textile was heat pressed at 160 °C for 30 s at 30 kPa.

Measurement and Evaluation of Printed Wiring: The surface and cross-section of printed traces were observed by laser microscope (VK-9710, KEYENCE Corp., Japan) and SEM (S4800, HitachiHighTechnologies with an accelerating voltage of 0.6-1 kV). The sheet resistance was calculated from printed line width and length which were measured from the microscope. Next, the printed textiles were stretched with a high precision mechanical system (AG-X, SHIMADZU Corp.) with a stretching speed of 15 mm min^{-1}, and the resistance was measured using the four-probes-method using a digital multisource meter (2400, Keithley Instruments Inc.), For cyclic test, the stretching and releasing speed was kept to 180 mm min^{-1}. The distance between electrodes was 30 mm while length of printed trace was 40 mm.

LED Integrated Textile: LED (LilyPad LED micro green, Sparkfun electronics) was attached to printed textile electrode with epoxy (Super-X 8008, CEMEDINE CO., Ltd.) and conductive epoxy (CW2400, CircuitWorks Co.). The voltage and current were applied and recorded by a semiconductor analyzer (B1500A, Agilent).

Wireless EMG Measurement Sleeve: A pair of electrode pads was printed on both front and back sides of the textile. Both sides of electrodes were connected through the permeation of the ink. Transmission lines were printed on front side to connect electrode pads and wireless module; the back side of transmission lines was covered by 50 µm thick thermoplastic polyurethane film (NSK Echomark, Japan) to prevent shorts caused by sweat. The wireless module (RF-ECG, Micro medical device, Inc.) and transmission lines were interconnected via snap button which was attached with conductive epoxy. Ag/AgCl gel electrodes (Ambu Blue Sensor SP Electrodes, Ambu) were used for control experiments. The diameter of each printed electrode was 1.5 cm which is same size with gel electrode. The distance between electrodes was 2 cm.

Four-Channel EMG Measurement Sleeve: Four pairs of electrodes were stencil printed to measure multiple EMG signals of forearm. The diameter of each electrode was 1 cm and distance between electrodes was 5 cm. Electrodes were connected to a medical electrical signal recording device (Neuropack S1, Nihon Kohden) via printed transmission lines. The gel electrode was set on the elbow as a virtual ground. The study protocol was thoroughly reviewed and approved by the ethical committee of the University of Tokyo (approval number KE14-25).

Washability Test: Washability of printed textile wiring was evaluated by machine wash warm (40 °C) normal 10–50 cycles and hang to dry, which is American Association of Textile Chemists and Colorists 135 1-III-B. Samples for washability test was prepared by printing five passes, heat pressing, and encapsulating with 50 µm TPU layer (NSK Echomark, Japan) for both sides.

Solvent Residue Analysis: Gas chromatography–mass spectrometry was conducted for checking the residue of BCA solvent. The sample was prepared with different drying times (1, 2, 5, 10 h at 90 °C) and the target analyte was extracted by acetone.

Supporting Information

Supporting Information is available from the Wiley Online Library or from the author.

Acknowledgements

This work was financially supported by the JST ERATO Bio-Harmonized Electronics Project. H. Jin was supported by Graduate Program for Leaders in Life Innovation (GPLLI). N. Matsuhisa was supported by Advanced Leading Graduate Course for Photon Science (ALPS) and the JSPS research fellowship for young scientists. The authors appreciate for fruitful discussions with Dr. Robert A. Nawrocki, Dr. David Ordinario, and Dr. Peter Zalar. The authors also appreciate Dr. Peter Zalar for editing the manuscript. The authors also wish to thank UTAX Co. Ltd. and Daikin Industries Co. Ltd for the materials used in this study.

Received: October 30, 2016
Revised: January 30, 2017
Published online: March 29, 2017

[1] M. Stoppa, A. Chiolerio, *Sensors* **2014**, *14*, 11957.
[2] M. Parrilla, R. Cánovas, I. Jeerapan, F. J. Andrade, J. Wang, *Adv. Healthcare Mater.* **2016**, *5*, 996.
[3] L. M. Castano, A. B. Flatau, *Smart Mater. Struct.* **2014**, *23*, 53001.

[4] J. Lee, H. Kwon, J. Seo, S. Shin, J. H. Koo, C. Pang, S. Son, J. H. Kim, Y. H. Jang, D. E. Kim, T. Lee, *Adv. Mater.* **2015**, *27*, 2433.
[5] W. Kim, S. Kwon, Y. C. Han, E. Kim, K. C. Choi, S.-H. Kang, B.-C. Park, *Adv. Electron. Mater.* **2016**, 1600220.
[6] Z. Zhang, K. Guo, Y. Li, X. Li, G. Guan, H. Li, Y. Luo, F. Zhao, Q. Zhang, B. Wei, Q. Pei, H. Peng, *Nat. Photonics* **2015**, *9*, 233.
[7] S. Takamatsu, T. Lonjaret, E. Ismailova, A. Masuda, T. Itoh, G. G. Malliaras, *Adv. Mater.* **2016**, *28*, 4485.
[8] T. Someya, T. Sekitani, S. Iba, Y. Kato, H. Kawaguchi, T. Sakurai, *Proc. Natl. Acad. Sci. USA* **2004**, *101*, 9966.
[9] T. Someya, Y. Kato, T. Sekitani, S. Iba, Y. Noguchi, Y. Murase, H. Kawaguchi, T. Sakurai, *Proc. Natl. Acad. Sci. USA* **2005**, *102*, 12321.
[10] M. Kaltenbrunner, T. Sekitani, J. Reeder, T. Yokota, K. Kuribara, T. Tokuhara, M. Drack, R. Schwödiauer, I. Graz, S. Bauer-Gogonea, S. Bauer, T. Someya, *Nature* **2013**, *499*, 458.
[11] G. A. Salvatore, N. Münzenrieder, T. Kinkeldei, L. Petti, C. Zysset, I. Strebel, L. Büthe, G. Tröster, *Nat. Commun.* **2014**, *5*, 3982.
[12] D.-H. Kim, N. Lu, R. Ma, Y.-S. Kim, R.-H. Kim, S. Wang, J. Wu, S. M. Won, H. Tao, A. Islam, K. J. Yu, T.-i. Kim, R. Chowdhury, M. Ying, L. Xu, M. Li, H.-J. Chung, H. Keum, M. McCormick, P. Liu, Y.-W. Zhang, F. G. Omenetto, Y. Huang, T. Coleman, J. a. Rogers, *Science* **2011**, *333*, 838.
[13] D. J. Lipomi, M. Vosgueritchian, B. C.-K. Tee, S. L. Hellstrom, J. a. Lee, C. H. Fox, Z. Bao, *Nat. Nanotechnol.* **2011**, *6*, 788.
[14] K.-Y. Chun, Y. Oh, J. Rho, J.-H. Ahn, Y.-J. Kim, H. R. Choi, S. Baik, *Nat. Nanotechnol.* **2010**, *5*, 853.
[15] M. Amjadi, A. Pichitpajongkit, S. Lee, S. Ryu, I. Park, *ACS Nano* **2014**, *8*, 5154.
[16] F. Xu, Y. Zhu, *Adv. Mater.* **2012**, *24*, 5117.
[17] A. Chiolerio, S. Bocchini, F. Scaravaggi, S. Porro, D. Perrone, D. Beretta, M. Caironi, C. Fabrizio Pirri, *Semicond. Sci. Technol.* **2015**, *30*, 104001.
[18] A. Chiolerio, P. Rivolo, S. Porro, S. Stassi, S. Ricciardi, P. Mandracci, G. Canavese, K. Bejtka, C. F. Pirri, *RSC Adv.* **2014**, *4*, 51477.
[19] M. Vosgueritchian, D. J. Lipomi, Z. Bao, *Adv. Funct. Mater.* **2012**, *22*, 421.
[20] S. Lee, A. Reuveny, J. Reeder, S. Lee, H. Jin, Q. Liu, T. Yokota, T. Sekitani, T. Isoyama, Y. Abe, Z. Suo, T. Someya, *Nat. Nanotechnol.* **2016**, *11*, 472.
[21] T. Yokota, Y. Inoue, Y. Terakawa, J. Reeder, M. Kaltenbrunner, T. Ware, K. Yang, K. Mabuchi, T. Murakawa, M. Sekino, W. Voit, T. Sekitani, T. Someya, *Proc. Natl. Acad. Sci. USA* **2015**, *112*, 14533.
[22] B.-S. Kim, S. W. Lee, H. Yoon, M. S. Strano, Y. Shao-Horn, P. T. Hammond, *Chem. Mater.* **2010**, *22*, 4791.
[23] K.-I. Jang, S. Y. Han, S. Xu, K. E. Mathewson, Y. Zhang, J.-W. Jeong, G.-T. Kim, R. C. Webb, J. W. Lee, T. J. Dawidczyk, R. H. Kim, Y. M. Song, W.-H. Yeo, S. Kim, H. Cheng, S. Il Rhee, J. Chung, B. Kim, H. U. Chung, D. Lee, Y. Yang, M. Cho, J. G. Gaspar, R. Carbonari, M. Fabiani, G. Gratton, Y. Huang, J. A. Rogers, *Nat. Commun.* **2014**, *5*, 4779.
[24] K. Cherenack, C. Zysset, T. Kinkeldei, N. Münzenrieder, G. Tröster, *Adv. Mater.* **2010**, *22*, 5178.
[25] Q. Li, X. M. Tao, *Proc. R. Soc. A: Math. Phys. Eng. Sci.* **2014**, *470*, 20140472.
[26] M. Varga, G. Tröster, Proc. of 2014 Int. Symp. on Wearable Computers Adjunct Program—ISWC'14 Adjunct, Association for Computing Machinery, New York, NY, USA, **2014**, p. 255.
[27] L. Hu, M. Pasta, F. La Mantia, L. Cui, S. Jeong, H. D. Deshazer, J. W. Choi, S. M. Han, Y. Cui, *Nano Lett.* **2010**, *10*, 708.
[28] Y. Ding, M. A. Invernale, G. A. Sotzing, *ACS Appl. Mater. Interfaces* **2010**, *2*, 1588.
[29] H.-W. Cui, K. Suganuma, H. Uchida, *Nano Res.* **2015**, *8*, 1604.
[30] Y.-H. Lee, Y. Kim, T.-I. Lee, I. Lee, J. Shin, H. S. Lee, T.-S. Kim, J. W. Choi, *ACS Nano* **2015**, *9*, 12214.
[31] I. Kazani, C. Hertleer, G. de Mey, A. Schwarz, G. Guxho, L. van Langenhove, *Fibres Text. East. Eur.* **2012**, *90*, 57.
[32] Y. Kim, H. Kim, H. J. Yoo, *IEEE Trans. Adv. Packag.* **2010**, *33*, 196.
[33] N. Matsuhisa, M. Kaltenbrunner, T. Yokota, H. Jinno, K. Kuribara, T. Sekitani, T. Someya, *Nat. Commun.* **2015**, *6*, 7461.
[34] Y. Tada, M. Inoue, T. Tokumaru, *J. Text. Inst.* **2014**, *105*, 692.
[35] K. Yang, C. Freeman, R. Torah, S. Beeby, J. Tudor, *Sens. Actuators, A* **2014**, *213*, 108.
[36] N. R. S. Hollies, M. M. Kaessinger, B. S. Watson, H. Bogaty, *Text. Res. J.* **1957**, *27*, 8.
[37] Q. Wang, B. Su, H. Liu, L. Jiang, *Adv. Mater.* **2014**, *26*, 4889.
[38] J. Yuan, X. Liu, O. Akbulut, J. Hu, S. L. Suib, J. Kong, F. Stellacci, *Nat. Nanotechnol.* **2008**, *3*, 332.